High-harmonic spectroscopy of isoelectronic molecules: Wavelength scaling of electronic-structure and multielectron effects

A. Rupenyan, P. M. Kraus, J. Schneider, and H. J. Wörner*
Laboratorium für Physikalische Chemie, ETH Zürich, Wolfgang-Pauli-Strasse 10, 8093 Zürich, Switzerland
(Received 27 September 2012; published 8 March 2013)

We study the interplay of electronic-structure and multielectron effects in high-harmonic spectra of the two isoelectronic molecules CO_2 and N_2O as a function of the near-infrared driving wavelength and intensity. We show that the minima observed in the spectra of aligned molecules ($\langle\cos^2\theta\rangle = 0.54$–$0.64$) are intensity dependent at the shortest investigated wavelength (1.17 μm) but become gradually intensity independent at longer wavelengths (1.36 and 1.46 μm). These results combined with detailed theoretical modeling show that the contributions of several ionization channels are important in the spectra recorded with short-wavelength driving pulses because the minima are located in the cutoff region where the contributions from different channels are comparable. In spectra recorded with longer driving wavelengths, the minima are located in the plateau region of the spectrum and are caused by the electronic structure of the molecules. Our results also rationalize and reconcile previous results and provide general guidelines for future studies.

DOI: 10.1103/PhysRevA.87.033409 PACS number(s): 33.20.Xx, 42.65.Ky, 42.50.Hz

I. INTRODUCTION

High-harmonic spectroscopy (HHS) relies on the interaction between a short, intense laser pulse and a molecule to access molecular structure and electronic dynamics on femtosecond to attosecond time scales [1–8]. The spectral amplitude and phase of the emitted high-harmonic radiation is sensitive to both the structure of the molecules and the induced dynamics. High-harmonic emission is successfully described as the consequence of the laser-field-induced photorecombination of an electron with a cation [9–12]. When the high harmonics are generated in aligned molecules, phenomena such as quantum interference, ionization to several electronic states of the cation and multielectron dynamics can be studied [13–20]. In spite of these important advances, the best-studied molecules N_2 and CO_2 still are the object of debates. Extending high-harmonic spectroscopy to more complex molecules thus requires detailed studies combining experimental data with theoretical modeling. This is the approach followed in the present article.

High-harmonic spectra contain information on the electronic structure of the target system, including Cooper minima [9,10], shape resonances [21], and two-center interference [13]. Such spectral structures result from the photorecombination of an electron with a cation in a well-defined electronic state, usually its electronic ground state. While Cooper minima and shape resonances are often known from photoionization experiments, two-center or Cohen-Fano interference minima have become more accessible through HHS because they are most clearly observed in aligned molecules. However, strong-field ionization of molecules can populate higher-lying electronic states in addition to the ground state of the cation [22]. The different states of the molecular ion populated between ionization and recombination provide different channels for high-harmonic emission. The ionization rate leading to a certain ionic state strongly depends on the binding energy, the shape, and the symmetry of the corresponding molecular orbital. Upon recombination, the resulting high-harmonic emission can be represented as a coherent sum of the emissions from multiple channels [16]. The relative phase of emission from two channels has a contribution proportional to the difference of the ionization potentials (I_p) $\Delta I_p \tau$ [23], where τ is the transit time of the electron in the continuum, and a contribution from the phase of the recombination dipole moment. When the interference between the emission of different channels is destructive, a minimum in the high-harmonic spectrum may be observed. By varying the intensity and wavelength of the generating laser pulses one can control the relative phase $\Delta I_p \tau$, which translates into a change in the position of the minimum [18]. This change has also been identified with the temporal evolution of an electronic wave packet in the cation created by ionization and probed by the photorecombination step. The observed minimum has thus been related to the attosecond dynamics of an electronic wave packet [16].

The interpretation of a minimum in high-harmonic spectra of CO_2 molecules has become a source of controversy in recent high-harmonic spectroscopy studies. Initially, a minimum in the spectrum of aligned CO_2 has been attributed to quantum interference in photorecombination [2,24]. However, the discovery of a dependence of the minimum position on the intensity and wavelength of the generating laser pulse has been successfully interpreted in terms of a destructive interference between emission from a channel involving the electronic ground state of the molecular cation, i.e., ionization from the highest-occupied molecular orbital (HOMO), and a channel involving the second excited state of the cation, i.e., ionization from HOMO-2. In the following, we will refer to spectral structures originating from a single channel as "structural" features. Minima resulting from the interference of emissions from multiple channels will be called "dynamical" to emphasize their relation to the continuum electron dynamics which is at the origin of their strong dependence on intensity and wavelength. The minimum in CO_2 has thus been reinterpreted as a dynamical rather than a structural feature [16], or the interplay of both dynamical and structural features [18,19].

*woerner@phys.chem.ethz.ch; www.atto.ethz.ch

More recently, a minimum observed in high-harmonic spectra generated at wavelengths of 1.45–1.70 μm has been attributed to structural effects [7] and spectra recorded at 1.3 μm have also been interpreted in terms of structural signatures [25].

In this article, we study the manifestations of electronic structure and multielectron effects in the high-harmonic spectra of the isoelectronic CO_2 and N_2O molecules. We address the recent controversy on the origin of the minimum in CO_2 and provide a clear physical picture explaining our observations, as well as the previous ones. Our experimental results bridge the wavelength gap between earlier measurements and demonstrate the gradual disappearance of multielectron effects with increasing wavelength of the probing field. The comparison of the experimental data with single-molecule calculations shows that the minimum in the high-harmonic spectra of aligned molecules with a typical degree of axis alignment $\langle\cos^2\theta\rangle = 0.54$–$0.64$ depends on the intensity of the driving field at the shortest investigated wavelength (1.17 μm) but gradually becomes intensity independent at longer wavelengths (1.36–1.46 μm). We note that these results are obtained using the same pulse durations in the multicycle regime (40–50 fs) and overlapping intensity ranges. We thus show that the observed transition from dynamical to structural signatures is not caused by different pulse lengths or intensities. The different observations at different wavelengths are rather a consequence of the minimum location relative to the cutoff of the high-harmonic spectrum and the different spectral shapes of the recombining photoelectron wave packets. At short wavelengths, the minimum is located closer to the cutoff where the contributions from several orbitals are comparable, whereas at longer wavelengths, the minimum is located in the plateau region of the spectrum where the contribution from the HOMO channel dominates. In addition, the observation of electronic structure or multielectron effects is also influenced by the alignment dependence of the high-harmonic emission in the cutoff region of the spectrum. Our results rationalize previous observations and provide a general physical picture that we expect to be useful in future studies of high-harmonic spectroscopy.

II. EXPERIMENTAL SETUP

The experimental setup consists of a chirped-pulse-amplified femtosecond Ti:sapphire laser system, a high-energy optical parametric amplifier (HE-TOPAS, Light Conversion) and a vacuum chamber for generation and spectral characterization of high-order harmonic radiation. The laser system (8 mJ, 25 fs, 1 kHz) provides pulses centered at 0.8 μm which traverse an 80:20 beam splitter. The major part is used to pump the TOPAS which generates tunable pulses with a wavelength between 1.1 and 2.4 μm and durations of 40–50 fs, measured by a home-built second-harmonic-generation frequency-resolved-optical-gating setup. These pulses are used to generate high-order harmonics with an intensity on target of 0.5–1.5×10^{14} W/cm^2, controlled using a neutral density filter. The minor part is stretched to 120 fs, with a peak intensity of 0.4×10^{13} W/cm^2 and is used to impulsively align the molecules in the gas jet. The IR probe beam is aligned parallel to the 0.8 μm alignment beam with a vertical offset of 0.7 cm and the two beams are focused into a gas jet inside a vacuum chamber using a $f = 50$ cm spherical mirror. The molecular beam is generated by supersonic expansion through a pulsed valve with a backing pressure of 5 bars. The focused probe beam intersects the molecular jet 1–3 mm downstream of the nozzle. This ensures that the probed molecules are sufficiently cooled for achieving high degrees of axis alignment. The best alignment obtained under these conditions and determined through comparison with our calculations amounts to $\langle\cos^2\theta\rangle = 0.64 \pm 0.01$. The high harmonics generated by the probe pulse propagate into an XUV spectrometer consisting of a 120-μm-wide entrance slit, a concave aberration-corrected grating (Shimadzu, 30-002) and an enhanced-dynamic-range microchannel-plate detector (Photonis, 37258) backed with a phosphor screen. A charge-coupled device camera records the spectral images and transfers them to a computer for analysis.

III. THEORETICAL MODEL

We calculate high-harmonic spectra by combining strong-field ionization rates from a velocity-gauge model [26,27], generalized in [16], with a returning photoelectron wave packet generated using the strong-field approximation [28] and photorecombination dipole moments from *ab initio* quantum scattering calculations. The valence electronic structure of CO_2 consists of the orbitals with the following symmetries and binding energies (equal to the vertical ionization energies within Koopmans' theorem): π_g, 13.78 eV; π_u, $\sim$17.59 eV; σ_u, 18.08 eV; σ_g, 19.40 eV [29]; and in N_2O the corresponding orbitals are π, 12.89 eV; σ, 16.38 eV; π, $\sim$18.2 eV; and σ, 20.11 eV [29]. The numbers quoted above are the vertical ionization energies measured by He I photoelectron spectroscopy. We used these numbers in our calculations. The binding energies of the four valence orbitals obtained in our MP2 calculations using a correlation-consistent polarized valence-triple-ζ (cc-pVTZ) basis set for CO_2 are 14.80, 19.44, 20.20, and 21.83 eV and the values obtained for N_2O are 13.24, 19.01, 20.71, and 22.83 eV.

When CO_2 is aligned parallel to the polarization of the generating laser field, both ionization from and recombination to HOMO are suppressed by the nodal plane of the orbital along the direction of tunneling [Fig. 1(a)]. However, the contribution from HOMO-2 is significant, due to its σ symmetry, although the ionization potential of HOMO-2 is higher than that of HOMO. Emission from HOMO-1 is suppressed, because of the presence of a nodal plane along the tunneling direction combined with its larger I_p. For N_2O, the corresponding relevant channels are HOMO and HOMO-1 [Fig. 2(a)], which is justified by the relative binding energies and angular variations of the ionization rates. The orbitals were obtained from Hartree-Fock calculations using a cc-pVTZ basis set. In this work, we use Hartree-Fock orbitals instead of the more appropriate Dyson orbitals [30–32] because the results do not differ significantly for the present work. The complex spectral representation of the induced dipole moment $d(\Omega,\theta)$ describing high-harmonic emission is a coherent sum containing the contributions of ionization from and recombination to the same orbital, as well as the propagation of the electron wave packet in the laser field. It can be expressed as follows [18,33,34] (atomic units are used throughout unless otherwise

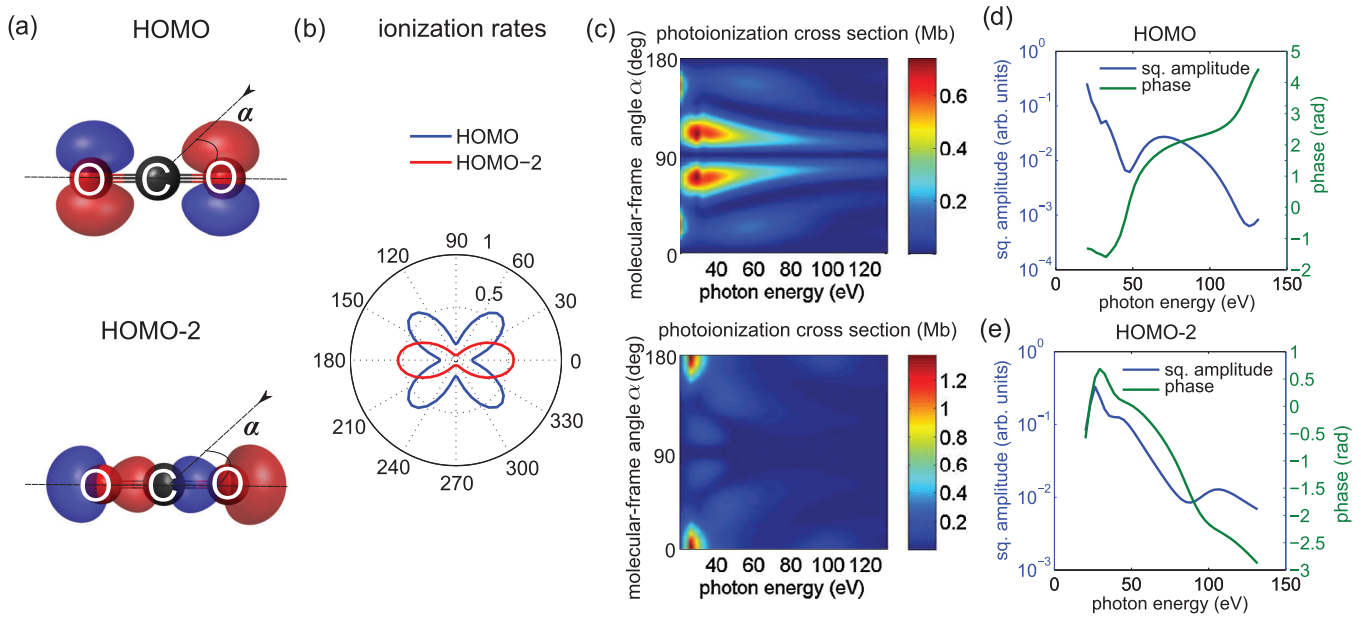

FIG. 1. (Color online) (a) Isoamplitude representations of the HOMO and HOMO-2 of CO_2 with color-coded sign from HF and cc-pVTZ calculations. (b) Angular variation of the strong-field ionization rates, calculated for an intensity of 1.0×10^{14} W/cm^2 and normalized to the ionization rate of a single atomic $1s$ orbital with the same ionization potential. (c) Molecular-frame photoionization cross sections calculated for HOMO (top panel) and HOMO-2 (bottom panel) using *ab initio* quantum scattering theory. (d) and (e) Squared amplitude and phase of the recombination dipoles of HOMO and HOMO-2 after multiplication with the ionization amplitudes and convolution with an axis distribution corresponding to $\langle \cos^2 \theta \rangle = 0.6$.

indicated):

$$d(\Omega,\theta) = \sum_i a_{ion,i}(\theta) a_{ewp,i}(\Omega) a_{rec,i}(\Omega,\theta), \qquad (1)$$

where the sum i runs over all molecular orbitals that are ionized in the laser field, Ω is the emitted frequency, and θ is the angle between the laser-field polarization and the molecular axis. The factor $a_{ion,i}(\theta)$ describes the angular variation of the strong-field ionization rate, $a_{ewp,i}(\Omega)$ represents the complex amplitude of the recombining photoelectron wave packet, depending on the wavelength, intensity, and pulse duration of the driving laser field, and $a_{rec,i}(\Omega,\theta)$ is the complex

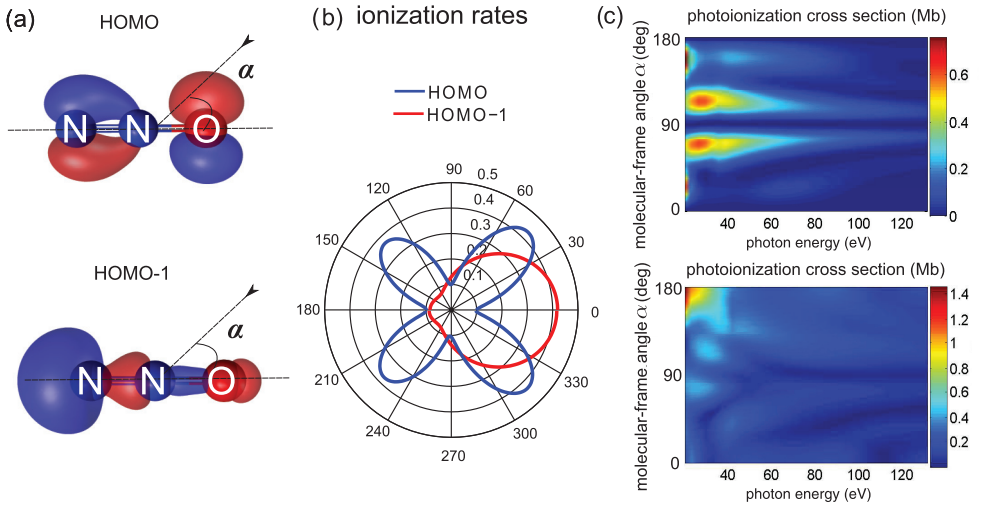

FIG. 2. (Color online) (a) Isoamplitude representations of the HOMO and HOMO-1 of N_2O with color-coded sign from HF and cc-pVTZ calculations. (b) Angular variation of the strong-field ionization rates, calculated for an intensity of 1.0×10^{14} W/cm^2 and normalized to the ionization rate of a single atomic orbital with the same ionization potential. (c) Molecular-frame photoionization cross sections calculated for the HOMO (top panel) and HOMO-1 (bottom panel) using *ab initio* quantum scattering theory.

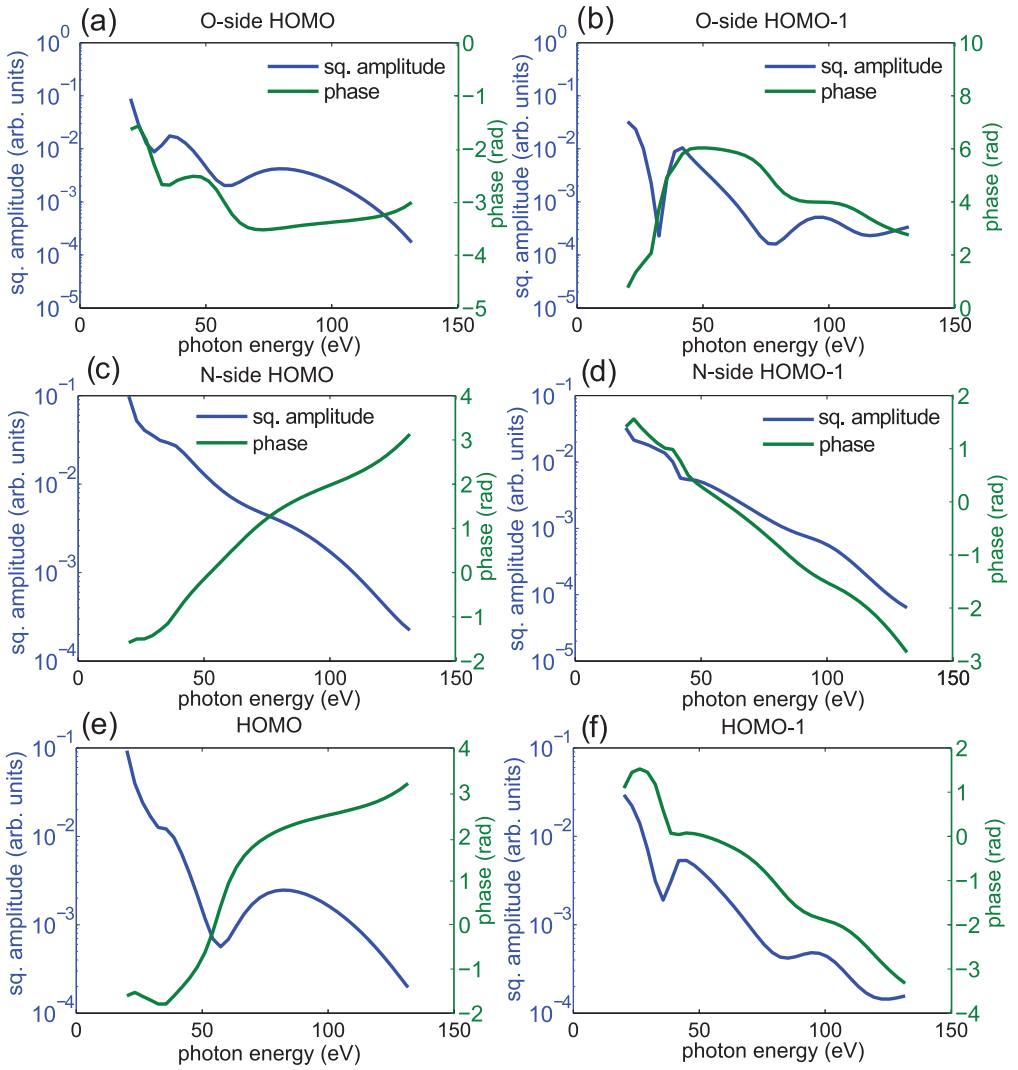

FIG. 3. (Color online) Channel- and recollision-side-resolved spectral amplitude and phase of high-harmonic emission from N_2O obtained by convoluting the product of ionization amplitudes and recombination dipoles of N_2O with an axis distribution corresponding to $\langle \cos^2 \theta \rangle = 0.6$. Panels (a) and (b) show the emission from the HOMO channel for recollision from the O and N side, respectively. Panels (c) and (d) show the same quantities for HOMO-1. Panels (e) and (f) show the total emission for HOMO and HOMO-1, respectively.

photorecombination matrix element. Classical photoelectron spectra of CO_2 and N_2O show that a very small change of the equilibrium geometry occurs when an electron is removed from HOMO or HOMO-2 of CO_2 and similarly for HOMO or HOMO-1 in N_2O. We therefore neglect nuclear motion during high-harmonic generation in our theoretical model.

Figure 1(a) shows the structure of the relevant orbitals of CO_2. We calculate the ionization rates $I_i(\theta)$ using a velocity-gauge model [16,26], and use $a_{ion,i}(\theta) \propto \sqrt{I_i(\theta)}$. The angular variations of the ionization rates, normalized to that of a single atomic orbital with the same I_p are shown in Fig. 1(b). The ionization rate of the HOMO is in good qualitative agreement with the results from the time-dependent Schrödinger equation obtained by Petretti *et al.* [35] and with the experimental results of Thomann *et al.* [36]. However, all three results, as well as further calculations, do not display the sharp angular variation obtained from a deconvolution of experimental data in Ref. [37]. The exponential I_p dependence of the ionization rate is contained in the amplitude of the electron wave packet $a_{ewp,i}(\Omega)$. The latter is obtained numerically using the strong-field approximation [28], with the laser parameters corresponding to our experimental conditions. The electron wave packet is obtained by Fourier transforming the calculated response using a smooth temporal filter to select the short trajectories. Our calculations use the nonadiabatic expressions of the tunnel-ionization rates [38] and fully include the effects of ionization depletion. The photorecombination matrix elements are obtained from *ab initio* quantum scattering calculations using EPOLYSCAT [39,40]. The differential photoionization cross sections for ionization from HOMO or HOMO-2 as a function of the emitted photon energy and the angle α between the molecular axis and the polarization of the photoionizing radiation is shown in Fig. 1(c).

The total induced dipole moment from an ensemble of molecules partially aligned along the direction of the

probe-field polarization is a coherent convolution of the induced dipole $d(\Omega,\theta)$ from single molecules aligned under an angle θ with respect to the generating field with the alignment distribution $A(\theta)$:

$$d(\Omega) = \sum_i a_{ewp,i}(\Omega) \times \int_0^\pi A_i(\theta) a_{ion,i}(\theta) a_{rec,i}(\Omega,\theta) \sin(\theta) d\theta. \quad (2)$$

The alignment distribution is parametrized using an analytical formula taken from [37]. Different degrees of alignment are represented using the parameters given in Ref. [41]. The resulting amplitude and phase of the induced dipole moment for each ionization channel is shown in Figs. 1(d) and 1(e) using $a_{ewp,i}(\Omega) = 1$ for clarity.

Several modifications need to be introduced to calculate high-harmonic emission from a noncentrosymmetric molecule such as N_2O and have been briefly described in Ref. [42]. First, in N_2O molecules partially aligned parallel to the laser polarization, the two contributing orbitals are HOMO and HOMO-1, shown in Fig. 2(a). We calculate the ionization rates of these orbitals using the velocity-gauge model and include the variation of the orbital binding energy with the angle between the molecular axis and the laser field arising from the Stark effect. We use the expression [43]

$$E = E_0 - \boldsymbol{\mu} \cdot \mathbf{F} - \frac{1}{2}\mathbf{F}^{\mathrm{T}} \underline{\underline{\boldsymbol{\alpha}}} \mathbf{F}, \quad (3)$$

where E_0 is the field-free binding energy of the orbital, $\boldsymbol{\mu}$ its permanent dipole moment, and $\underline{\underline{\boldsymbol{\alpha}}}$ its polarizability tensor. These quantities are obtained from *ab initio* quantum chemical calculations using the MP2 method with a cc-pVTZ basis set. The total dipole moment of N_2O at this level of theory is 0.209 D, which is in reasonable agreement with the experimental value of 0.167 D. Such calculations are performed with an applied static electric field in the range $F = 0$–0.1 a.u. and Eq. (3) is fitted to the obtained binding energies. The results of these calculations are shown in Fig. 2(b). The ionization rate of the HOMO is almost inversion symmetric, owing to its small permanent dipole moment, whereas the ionization rate of the HOMO-1 has a pronounced asymmetry that is dominated by the Stark effect. The ionization rate is found to maximize when the electric field points from the O to the N end of the molecule, i.e., in the direction of the permanent dipole moment of the orbital, thus favoring removal of the electron via the O end of the molecule.

We now separately study the predicted high-harmonic emission for electron recombination from the two opposite

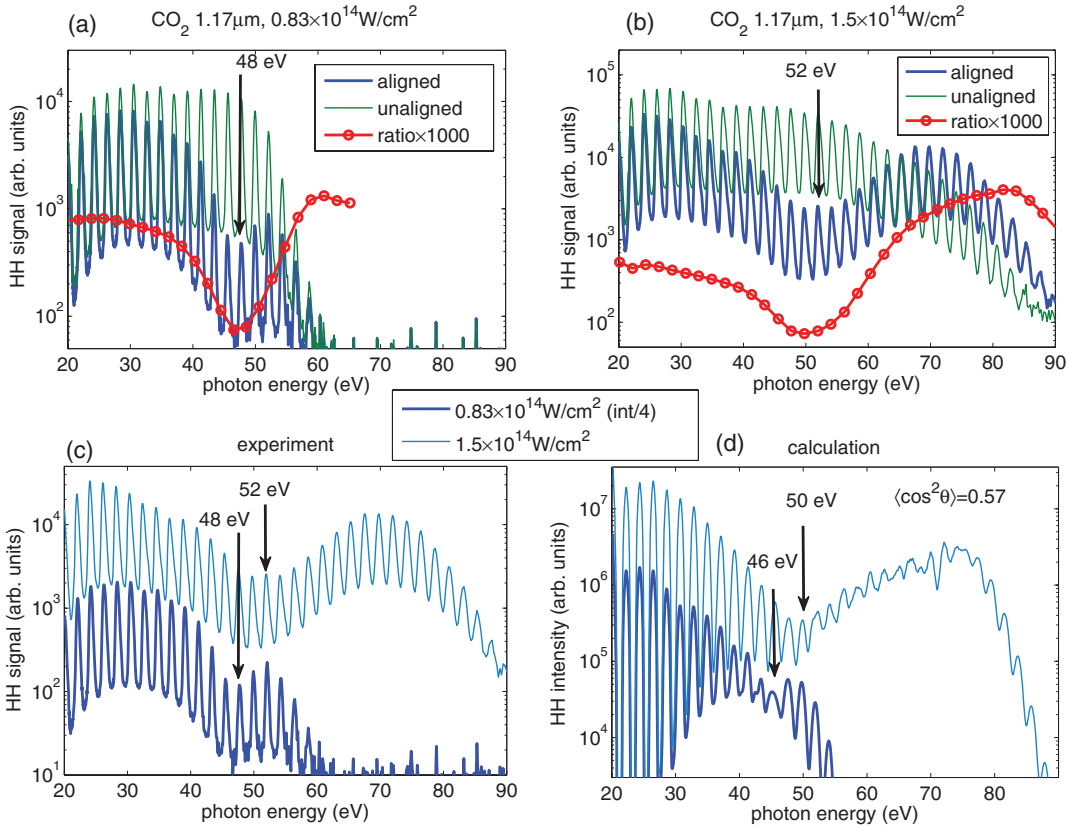

FIG. 4. (Color online) Experimental high-harmonic spectra generated in CO_2 molecules using 40 fs laser pulses centered at 1.17 μm. Panels (a) and (b) show spectra generated in transiently aligned molecules (thick blue line), unaligned molecules (thin green line), and their ratio (red circles), recorded at different intensities given above each panel. Panel (c) shows the spectra recorded in transiently aligned molecules on a common scale and panel (d) shows the calculated high-harmonic spectra reproducing the experimental high-harmonic spectra from panel (c), indicating the determined degree of alignment.

sides of the N_2O molecule. To account for the the lack of inversion symmetry, we split the integral in Eq. (2) into two parts from 0° to 90°, and from 90° to 180°. When we integrate over angles $\alpha = 0°$–$90°$, accounting for an electron recolliding from the O side of the molecule we observe two minima in the spectrum, a narrow minimum at 29 eV, and a broader minimum, similar to the minimum in CO_2 [Fig. 1(d)], at 59 eV, shown in Fig. 3(a). When we integrate over angles $\alpha = 90°$–$180°$, corresponding to recombination from the N side of the molecule, the resulting spectrum shown in Fig. 3(b) is almost structureless. A similar result is obtained for the emission from HOMO-1, shown in Figs. 3(c) and 3(d), where two pronounced minima in the harmonic intensity are found when recollision happens from the O side [Fig. 3(c)], whereas no minima are seen when recombination happens from the N side of the molecule [Fig. 3(d)]. As N_2O is noncentrosymmetric, the difference in the harmonic spectra emitted upon recombination from the N side or the O side is a consequence of the diffraction of the returning photoelectron wave in the asymmetric molecular potential. We note, that this result fundamentally differs from the plane-wave approximation where the photorecombination dipole moments for recollision from the two sides would simply be complex conjugates of each other [44–46]. The calculated spectrum emitted from HOMO shown in Fig. 3(e), results from the coherent summation of the emission from the two sides of N_2O and is characterized by the disappearance of the small minimum at 29 eV in Fig. 3(a), and the enhancement of the minimum at 59 eV. In the total amplitude of HOMO-1, shown in Fig. 3(f), both minima are preserved, although they are somewhat shallower and shifted to higher photon energies by 3–4 eV.

IV. RESULTS

We study high-harmonic spectra of aligned CO_2 and N_2O molecules by impulsively aligning the molecules with an intense nonresonant laser pulse and generating high harmonics with probe pulses of different wavelengths and intensities. The following measured harmonic spectra are recorded at the delay between the aligning and generating pulses that corresponds to maximal alignment within the first half revival of the rotational dynamics, i.e., 21.1 ps in CO_2 and 19.7 ps in N_2O.

Figures 4 and 5 show high-harmonic spectra of CO_2 and N_2O, recorded with laser pulses centered at 1.17 μm and different intensities indicated in the legends. Here and in the remainder of this article, the peak intensities were determined by matching the cutoff of the calculated spectra to the experimental results. Panels (a) and (b) of both figures show spectra generated in molecules aligned parallel to the polarization of the probe field (thick blue lines), in randomly aligned molecules (thin green lines), and their ratio (red circles). All spectra of aligned molecules show a pronounced minimum which is also visible in the ratios. The spectra are reproduced on a common scale in panel (c). In both molecules, we observe a shift of the minimum to higher photon energies with increasing intensity of the probe field. In CO_2 the minimum is found to shift from 48 to 52 eV, and in N_2O the minimum shifts from 50 to 55 eV. The degree of alignment in these measurements, determined by comparison with our simulation is $\langle\cos^2\theta\rangle = 0.57$ for CO_2 molecules and $\langle\cos^2\theta\rangle = 0.63$ for N_2O molecules. A higher degree of alignment is indeed expected for N_2O when the two molecules are exposed to the same alignment pulses [42]. The minima in the ratios are systematically located at 1–3 eV

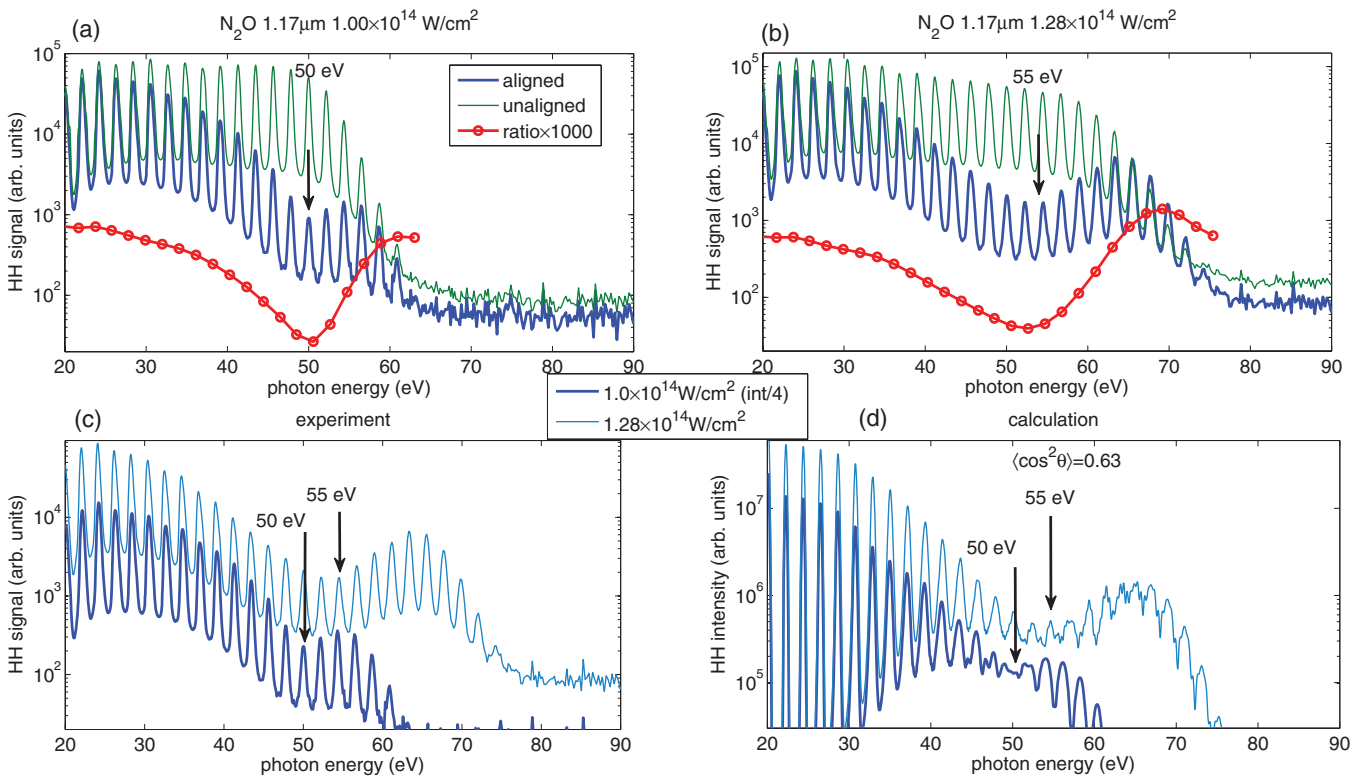

FIG. 5. (Color online) Same as Fig. 4 with experimental spectra recorded in N_2O using 40 fs laser pulses centered at 1.17 μm.

lower photon energies than the minima in the spectra of aligned molecules. This is a consequence of the decreasing intensity with increasing photon energy in the spectrum of the randomly aligned molecules. For theoretical modeling, it is thus important to calculate the appropriate quantity when comparing to experimental results. Panel (d) shows the calculated spectra, obtained from simulations using generating pulse parameters (intensity, duration, and central wavelength) that match the experimental conditions of the measurements shown in panels (a)–(c) of Figs. 4 and 5. The degree of alignment was determined independently for measurements done at different wavelengths because the properties of the infrared probe beam change slightly with wavelength. However, when only the intensity of the probe pulse changes, the degree of alignment is assumed (and found) to be constant. Our model successfully reproduces the 4 eV shift of the minimum position, observed in the experimental data of CO_2 shown in Fig. 4(c), and the shift of the minimum position from 50 to 55 eV observed in the experimental data of N_2O, shown in Fig. 5(c).

Figure 6 shows high-harmonic spectra recorded in CO_2 molecules with 40-fs laser pulses centered at 1.36 μm and different intensities given in the legend. Panels (a) and (b) show spectra generated in molecules aligned parallel to the polarization of the probe field (thick blue lines), in randomly aligned molecules (thin green lines), and their ratio (red circles). Panel (c) reproduces the spectra generated in aligned molecules on a common scale. The minima in the spectra of aligned CO_2 molecules are found at 54 eV and the minima in the ratios are found at 52 eV. In contrast to the results obtained at 1.17 μm (Fig. 4), the position of the minima is independent of the intensity of the probe pulses. The degree of alignment, determined by comparing the experiment with the simulations, is $\langle \cos^2 \theta \rangle = 0.54$. The calculated spectra, shown in panel (d), again accurately reproduce the experimental ones, and show that the minimum position remains the same for different intensities of the generating pulse.

Similar measurements recorded with a central wavelength of 1.46 μm and a pulse duration of 40 fs are shown in Fig. 7. The minimum in the spectra of aligned molecules is found at 47 eV and the minimum in the ratios is at 46 eV. By comparison with our simulations, we have determined the degree of alignment to be $\langle \cos^2 \theta \rangle \approx 0.59$. As in the case of a central wavelength of 1.36 μm (Fig. 6), the position of the minima is found to be independent of the intensity of the probe pulses. The intensity independence of the minimum at this central wavelength is reproduced in the calculated spectra, shown in panel (d). We note that in CO_2 the emission from aligned molecules extends to higher photon energies than that from unaligned molecules, especially for the higher intensities of the generating field. This is also the case in Figs. 4 and 6. This effect is also present in N_2O but is less pronounced. We will show below that this observation results from the alignment dependence of emission from HOMO [see Fig. 14(a)]. Spectra of aligned CO_2 molecules recorded with a

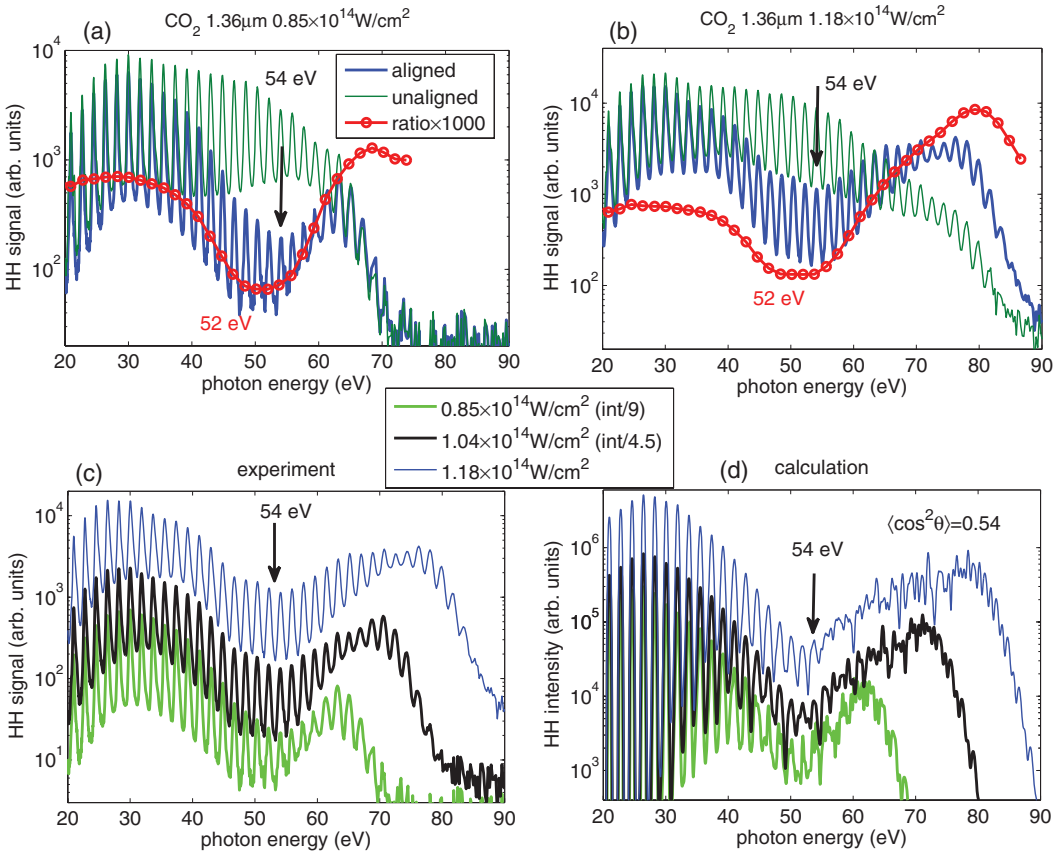

FIG. 6. (Color online) Same as Fig. 4 with experimental spectra recorded in CO_2 using 40 fs laser pulses centered at 1.36 μm.

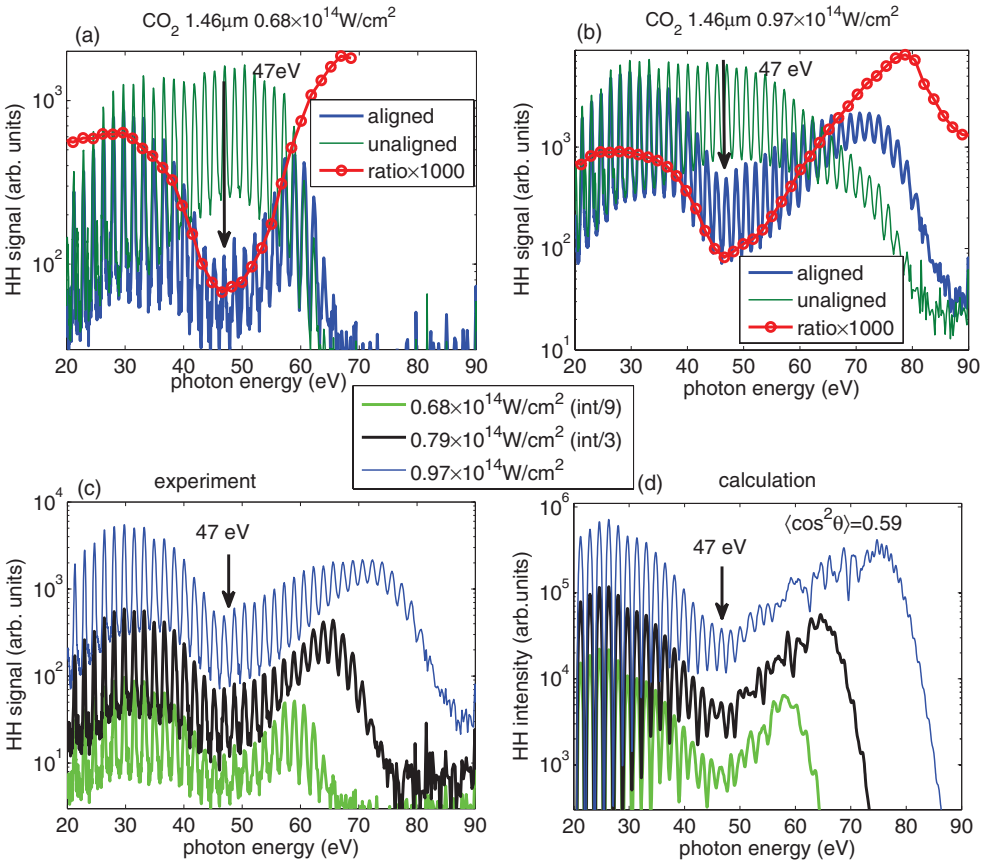

FIG. 7. (Color online) Same as Fig. 4 with experimental spectra recorded in CO_2 using 40 fs laser pulses centered at 1.46 μm.

central wavelength of 1.45 μm have been reported in Ref. [7], however using much shorter laser pulses than in the present study. We will return to this point in Sec. V.

Figures 8 and 9 show measurements similar to Figs. 5 and 6, but recorded in N_2O molecules. Figure 8 shows measurements performed with a central wavelength of 1.36 μm. The minima in the spectra of aligned molecules are located at 52–54 eV and the minima in the ratios are found at 1–3 eV lower photon energies. The degree of alignment determined by comparison with the calculations is $\langle\cos^2\theta\rangle = 0.64$. The observed shift of the minimum position between the lowest and highest intensity in Fig. 8 is close to 2 eV, and is approximately reproduced in the calculations shown in Fig. 8(d). The minimum position is also found at 53–54 eV in the spectra recorded using a wavelength of 1.46 μm, shown in Figs. 9(a)–9(c). The degree of alignment is found to be the same as in Fig. 8. The shift in the position of the minima is less than 1 eV. The calculated spectra, shown in panel (d), for a driving wavelength of 1.46 μm reproduce the measured ones, although no shift in the position of the minimum is observed.

We further investigate high-harmonic spectra of aligned CO_2 and N_2O molecules, recorded under identical conditions for the two molecules in Fig. 10. The positions of the minima in the spectra are indicated by arrows. In Fig. 10(a) the minimum in the CO_2 spectrum generated at 1.19 μm is located at 52 eV, whereas it is at 57 eV in the N_2O spectrum. In the spectra recorded at 1.3 and 1.46 μm, shown in Figs. 10(b) and 10(c), the minima in the N_2O spectra are located at 8 and 5 eV higher photon energies, respectively, than in the corresponding CO_2 spectra. This difference in the position of the minima is the result of the fact that N_2O is noncentrosymmetric, more polarizable, and characterized by different ionization rates and recombination dipoles. We have shown by numerically solving the time-dependent Schrödinger equation, that when exposed to the same alignment pulse, N_2O reaches values of $\langle\cos^2\theta\rangle$ that exceed those achieved in CO_2 by ~0.05 [42]. Our calculations of high-harmonic spectra further showed that for identical axis distributions, the structural minimum in the HOMO emission spectrum of N_2O molecules is located at 10 eV higher photon energy than the minimum in the spectrum of CO_2 molecules, which is a consequence of the electronic structure of N_2O compared to CO_2 as discussed in [42]. The smaller separation of the centers of gravity of the HOMO electron density in N_2O compared to CO_2 causes the minimum to occur for a shorter de Broglie wavelength of the recombining electron and thus for a higher photon energy. When the two molecules are exposed to the same alignment pulse, the difference in the positions of the minima is reduced to 5–8 eV because N_2O aligns more strongly, which moves the minimum to lower photon energies. This result, obtained in Ref. [42] using a wavelength of 1.46 μm is confirmed here at 1.3 μm. At 1.19 μm, the difference between the minimum positions is additionally affected by the interference of emission from HOMO with that from HOMO-2 in CO_2 and HOMO-1 in N_2O, but the minimum in N_2O is still found to occur 5 eV below that of CO_2.

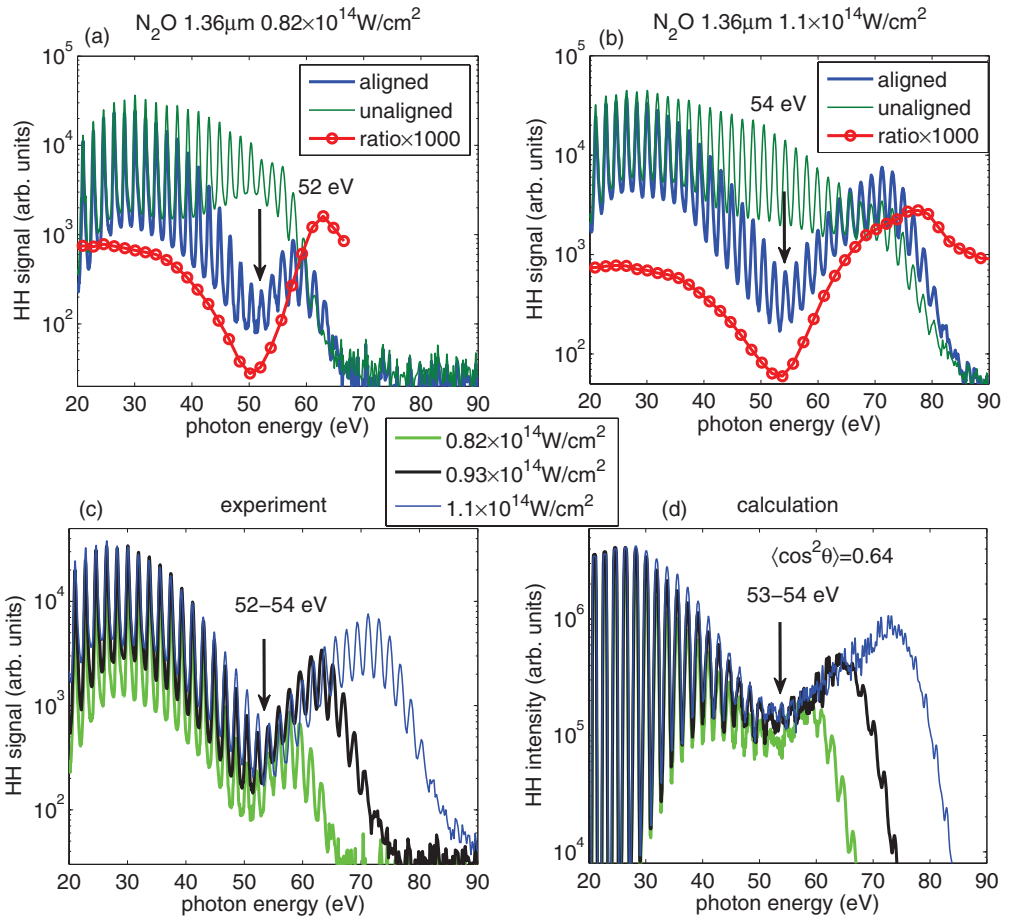

FIG. 8. (Color online) Same as Fig. 4 with experimental spectra recorded in N_2O using 40 fs laser pulses centered at 1.36 μm.

V. DISCUSSION

Our experiments show that the position of the minimum in the spectra of aligned CO_2 and N_2O molecules shifts to higher photon energies with increasing intensity when 1.17 μm probe pulses are used. For longer wavelengths (1.36 and 1.46 μm), the observed shift in the spectra of N_2O molecules is considerably smaller, and inexistent in the spectra of CO_2 molecules. A shift in the position of the minimum with intensity in CO_2 has previously been interpreted as a multielectron effect, resulting from interference between high-harmonic emission from the HOMO and HOMO-2 [16,18,19]. The more gradual disappearance of multielectron effects in N_2O with increasing wavelength is expected, since the difference in ionization potentials of the two contributing channels is smaller in N_2O (3.5 eV) than in CO_2 (4.3 eV). The model that we have outlined above reproduces the positions of the minima observed under all experimental conditions with an accuracy of better than 2 eV.

The minimum observed at wavelengths of 1.45 μm and longer in Ref. [7] has not shown any intensity dependence, and has been attributed to destructive quantum interference related to the orbital structure of CO_2. We confirm this observation here and note that our degree of alignment must be substantially higher than in Ref. [7], given the lower position of the minimum in photon energy. The minimum in the high-harmonic spectra shown in Ref. [7] is at 60 eV, whereas in the measurements presented in this article (Figs. 4, 6, 7), it is found at 47–54 eV, corresponding to $\langle\cos^2\theta\rangle = 0.59$–$0.54$. This implies that the degree of alignment in Ref. [7] was lower than in the present experiments. We further study this aspect in Figs. 14 and 15 below. The absence of multielectron effects in the measurements of Ref. [7] has been attributed to the use of shorter laser pulses compared to Refs. [18,19]. The authors of Ref. [7] speculated that the occurrence of a dynamic minimum requires a quasiadiabatic generation condition, otherwise the intensity-dependent destructive interference of different harmonic-generation channels would be averaged out over the duration of the driving pulse. We have used longer near-IR laser pulses with a duration of 40–50 fs (eight to ten optical cycles, compared to three to four optical cycles in [7]), but still observe an intensity-independent minimum in CO_2 at 1.46 μm. This result and our theoretical analysis clearly show that the observed minimum is a feature of the emission from the HOMO channel, rather than a consequence of interference between contributions from different channels.

We now use our theoretical model to analyze and rationalize these findings. Several factors influence the position of the minimum: the wavelength of the generating laser pulses, their intensity, and the degree of alignment of the molecules. We will determine the effect of each of these factors separately. We first study the effect of the wavelength. Figure 11 shows the channel-resolved contributions to the high-harmonic emission spectrum calculated using laser pulses with different central wavelengths but the same peak intensity (0.8×10^{14} W/cm^2)

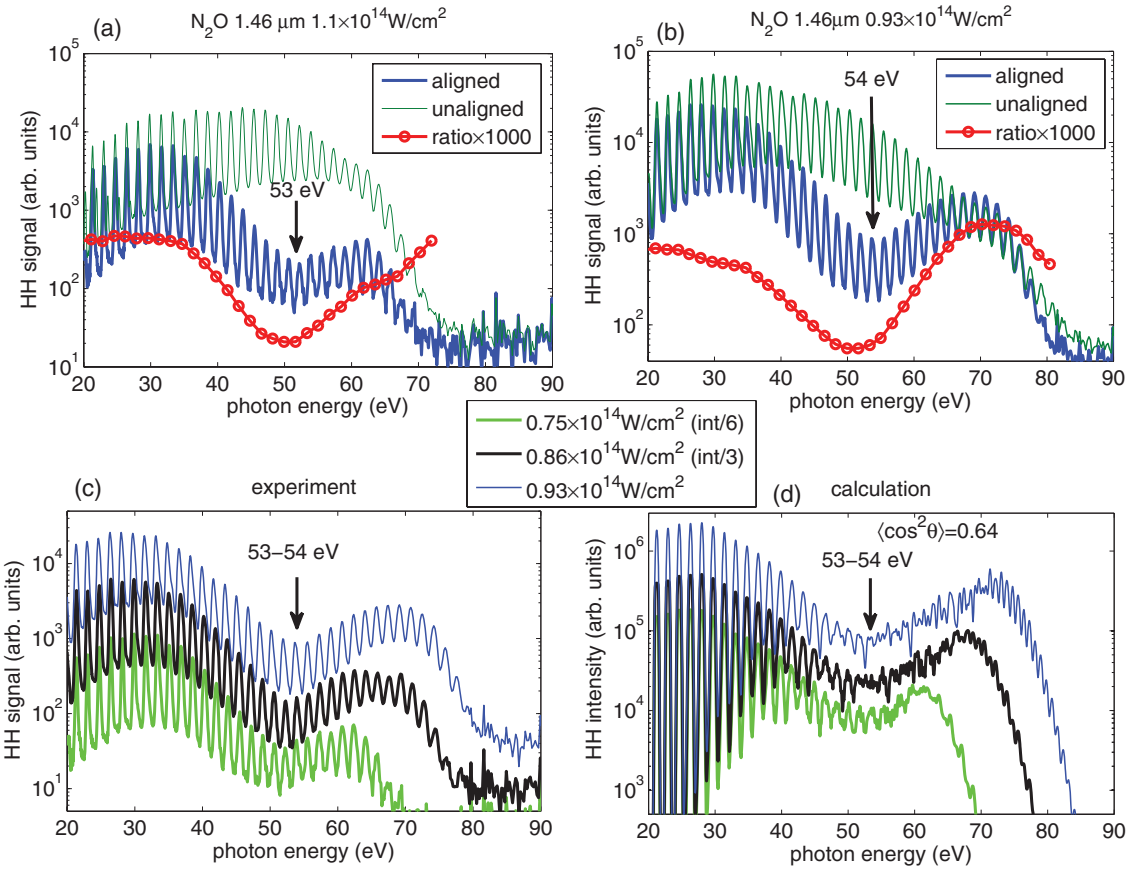

FIG. 9. (Color online) Same as Fig. 4 with experimental spectra recorded in N_2O using 40 fs laser pulses centered at 1.46 μm.

and duration (40 fs). The intensity of the emission from HOMO-2 is comparable to that of HOMO in the cutoff for all wavelengths. However, the extension of the cutoff decreases with increasing wavelength and therefore the range of harmonics with comparable contributions from multiple channels is also reduced. This result is explained by the combined effect of the smaller number of optical cycles contained in longer-wavelength pulses and the intensity dependence of the relative ionization rates of the two channels. In the long-wavelength pulses, ionization is confined to a smaller number of optical cycles with larger intensity differences between consecutive cycles. The temporal confinement of emission explains the larger extent of the plateau relative to the cutoff at longer wavelengths. The larger intensity differences between consecutive cycles explains the observed overall suppression of HOMO-2 emission with increasing wavelength. We have also found that the calculated strong-field ionization yield of HOMO-2 decreases with increasing wavelength for the results shown in Fig. 11. The results in Fig. 11 thus show that the minimum in the spectra recorded at 1.3 μm and longer wavelengths originates from the HOMO channel rather than from the interference of the two dominant channels. Under the conditions adopted in these calculations, one can thus expect to observe intensity-dependent minima resulting from interference for wavelengths of 0.8–1.2 μm but intensity-independent structural minima at 1.3 μm and longer wavelengths, as we have indeed observed.

We now investigate the effect of the intensity of the generating pulse on the high-harmonic spectra. To validate our model further, we simulate high-harmonic spectra of aligned CO_2 molecules using a wavelength of 0.8 μm and different intensities. Figures 12(a) and 12(b) show the calculated channel-resolved spectra of aligned CO_2 molecules, using intensities of 1.0×10^{14} W/cm^2 and 1.6×10^{14} W/cm^2, respectively. The structural minimum in the HOMO channel is barely visible because of the rapid intensity decrease in the cutoff region. The coherent addition of the emission from the two channels results in a minimum visible in the harmonic ratios [Fig. 12(c)]. The minimum is located at H23 (35.6 eV) for the lower intensity, whereas it is shifted to H27 (42.2 eV) for the higher intensity. This shows that our model reproduces the intensity dependence of the minimum position reported in experiments at 0.8 μm [16] and supports the interpretation of the spectral minimum as a dynamic feature, resulting from the interference of emission from HOMO and HOMO-2. Figure 13 shows calculated high-harmonic spectra of aligned N_2O molecules using a wavelength of 1.2 μm. The intensities of HOMO and HOMO-1 emission are comparable in the cutoff region, for an intensity of 0.6×10^{14} W/cm^2 shown in panel (a). For the higher laser intensity (1.4×10^{14} W/cm^2) shown in panel (b), the HOMO-1 contribution is considerably smaller in the cutoff and a minimum at H49 (50.8 eV) is present in the total emission. This minimum is preserved in the harmonic ratios [Fig. 13(c)], whereas the position of

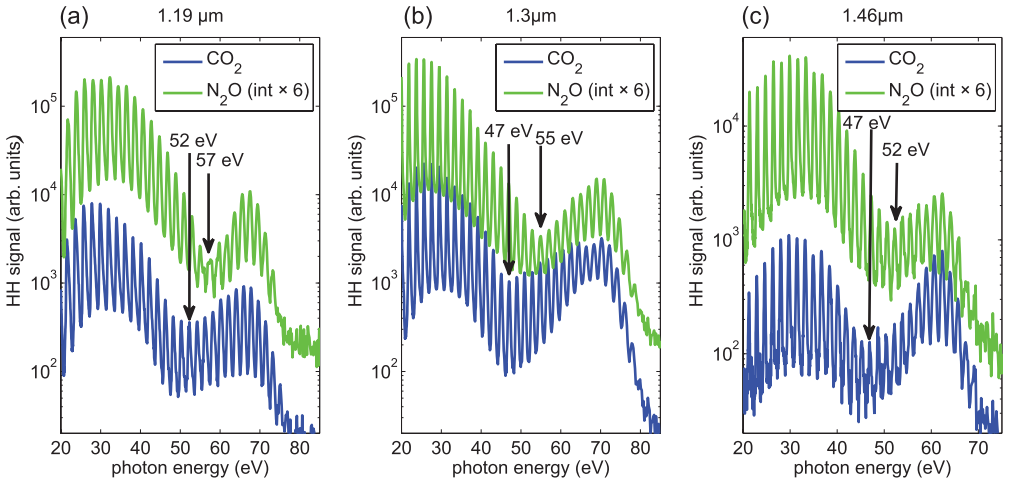

FIG. 10. (Color online) Measured high-harmonic spectra generated in transiently aligned N_2O and CO_2 molecules under identical experimental conditions using a generating pulse of central wavelength 1.19 μm (a), 1.3 μm (b), or 1.46 μm (c). The results show that the spectral minimum measured in N_2O is always located at higher photon energies compared to CO_2 under identical experimental conditions.

the minimum in Fig. 13(a) is 5 eV lower, at H45 (46.4 eV). In analogy with the simulations at 0.8 μm, the minimum at the lower photon energy therefore originates from destructive interference between emission from HOMO and HOMO-1. At the higher intensity of the driving field, the total emission has inherited the features of the HOMO emission alone, which shows that the minimum at 51 eV is a signature of the electronic structure, in contrast to the dynamic minimum observed at lower intensities. Thus, the high-harmonic spectra generated using laser pulses centered at 1.2 μm show both dynamic and/or structural effects, depending on the intensity of the laser field [18].

We now turn to the effect of the degree of alignment on the position and intensity dependence of the spectral minima. The channel-resolved spectral envelopes of emission from HOMO and HOMO-2 in CO_2 are shown in Figs. 14(a) and 14(b). Figures 14(c) and 14(d) show the spectral envelopes of the HOMO and HOMO-1 emission for N_2O molecules. For the same intensity and wavelength, varying the degree of alignment results in a shift of the position of the minimum

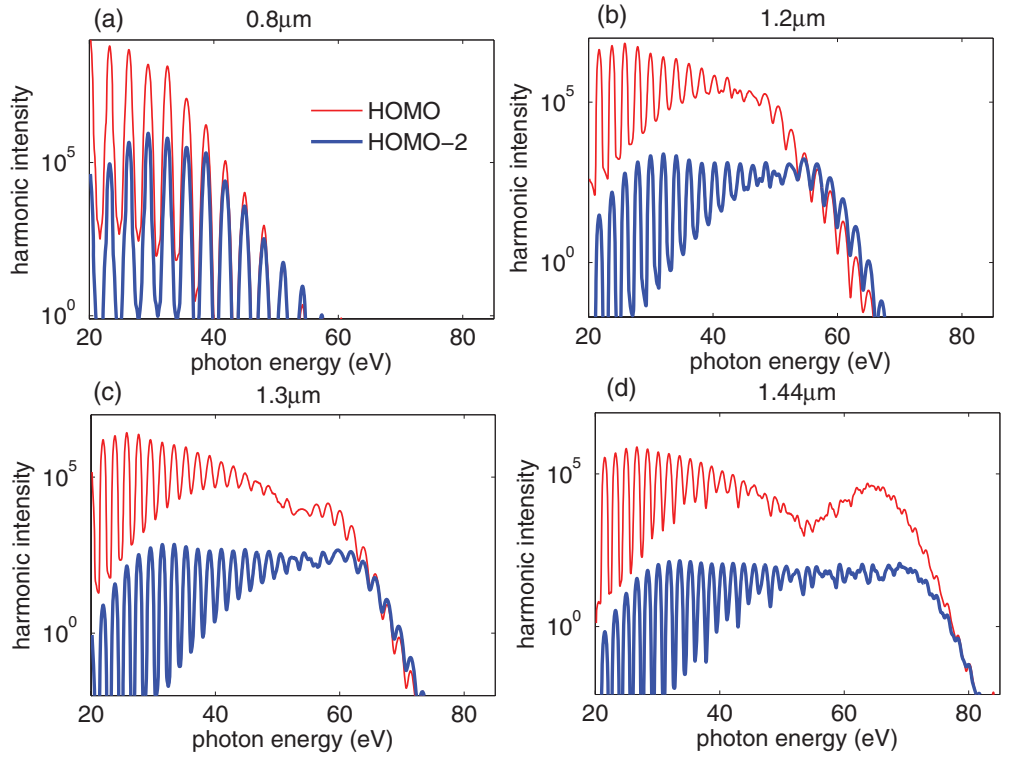

FIG. 11. (Color online) Calculated channel-resolved high-harmonic spectra for aligned CO_2 molecules ($\langle\cos^2\theta\rangle = 0.5$), at different central wavelengths indicated above each panel, using a constant pulse length (40 fs) and intensity (0.8×10^{14} W/cm^2).

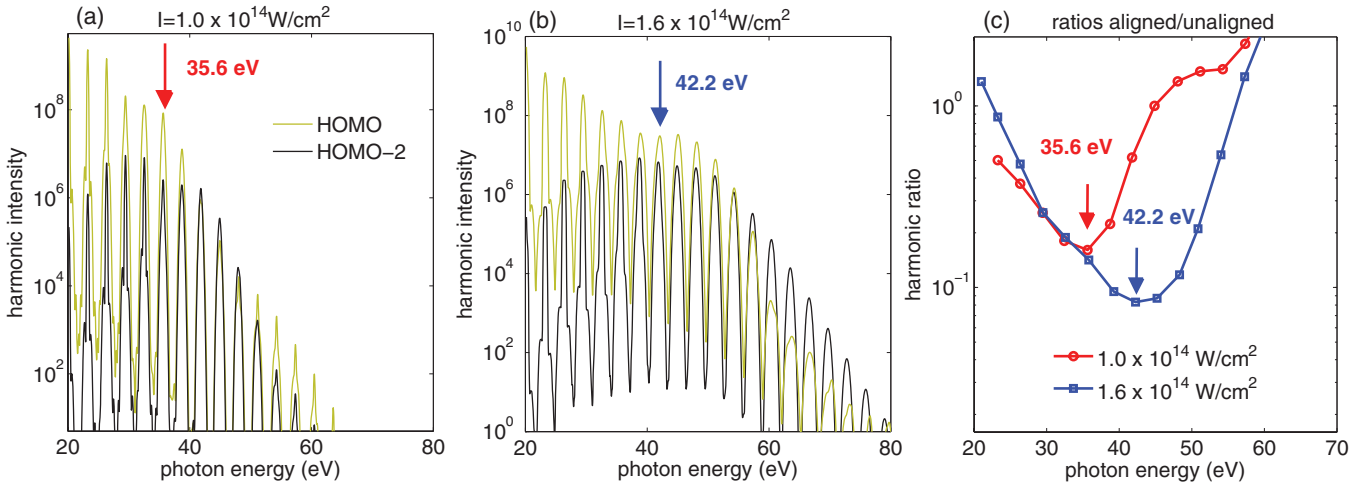

FIG. 12. (Color online) Calculated channel-resolved high-harmonic spectra of aligned CO_2 molecules ($\langle\cos^2\theta\rangle = 0.65$) using 40 fs, 0.8 μm laser pulses with intensities of 1.0×10^{14} W/cm^2 (a) and 1.6×10^{14} W/cm^2 (b). Panel (c) shows the ratio of the total emitted intensity of aligned CO_2 molecules to that of unaligned molecules. The position of the minima in the ratios is also indicated in panels (a) and (b).

in CO_2, in agreement with Ref. [47]. This result is expected from the point of view of quantum interference. A higher degree of alignment corresponds to a narrower axis distribution and therefore to a larger effective extension of the molecular orbital along the direction of the returning electron. Destructive interference thus occurs at longer de-Broglie wavelengths, i.e., lower photon energies. Both the shape of the spectra and that of the minimum change with the degree of alignment. When the degree of alignment is high, the HOMO emission from both CO_2 and N_2O is suppressed for photon energies below the minimum, but enhanced for photon energies above the minimum. Under the same conditions the emission from HOMO-2 of CO_2 is enhanced over the whole spectral range. This change of the spectral envelope also influences the dominance of structural or dynamical effects. For low degrees of alignment, the HOMO emission in the cutoff region is more suppressed than that of HOMO-2, which favors the observation of a dynamic minimum. This can indeed be seen in Figs. 11(a) and 11(b) where the contribution of HOMO-2 is comparable to that of HOMO in the cutoff because of the relatively low degree of alignment ($\langle\cos^2\theta\rangle = 0.5$). For higher degrees of alignment, the emission from HOMO is enhanced in the cutoff region such that interference with emission from HOMO-2 becomes less important. A similar situation has been described in N_2, where the contribution from HOMO-1 was found to be important in the cutoff [14]. The strong enhancement of the HOMO emission in the cutoff has also been observed experimentally, e.g. in Figs. 6(b) and 7(b) where the emission from aligned CO_2 molecules dominates strongly over the emission from randomly aligned molecules. The different strengths of alignment dependence in HOMO and HOMO-2 emissions also rationalizes the observation of an intensity dependence of the minimum position in spectra recorded at 1.3 μm reported in Ref. [19]. According to our analysis of the spectra reported in [19], the degree of alignment was low ($\langle\cos^2\theta\rangle = 0.46 \pm 0.02$),

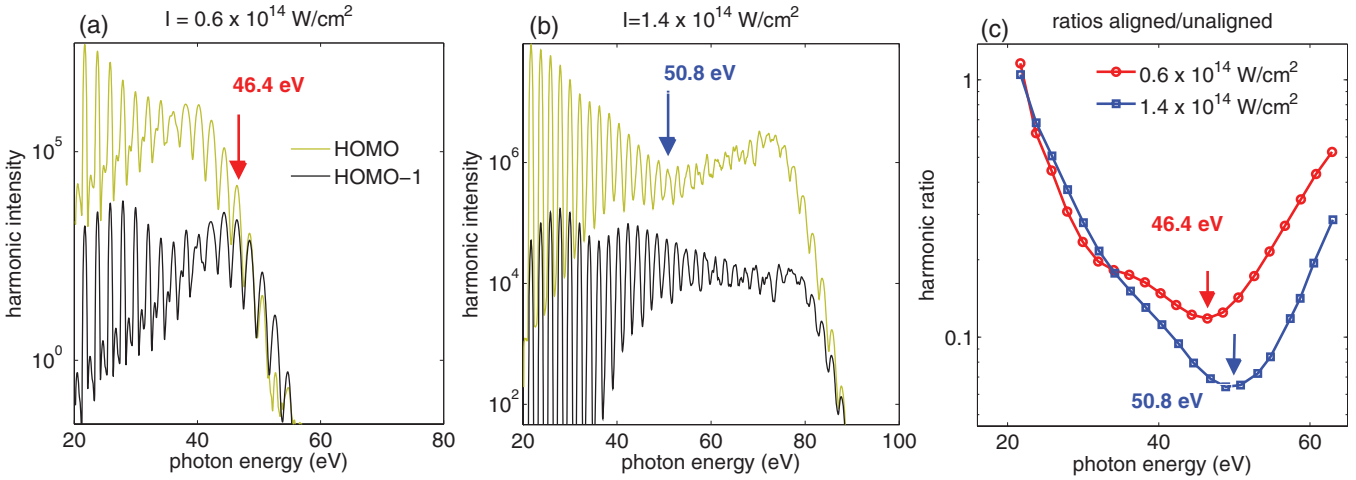

FIG. 13. (Color online) Calculated channel-resolved high-harmonic spectra of aligned N_2O molecules ($\langle\cos^2\theta\rangle = 0.65$) using 40 fs, 1.2 μm laser pulses with intensities of 0.6×10^{14} W/cm^2 (a) and 1.4×10^{14} W/cm^2 (b). Panel (c) shows the ratio of the total emitted intensity to that of unaligned N_2O molecules. The position of the minima in the ratios is also indicated in panels (a) and (b).

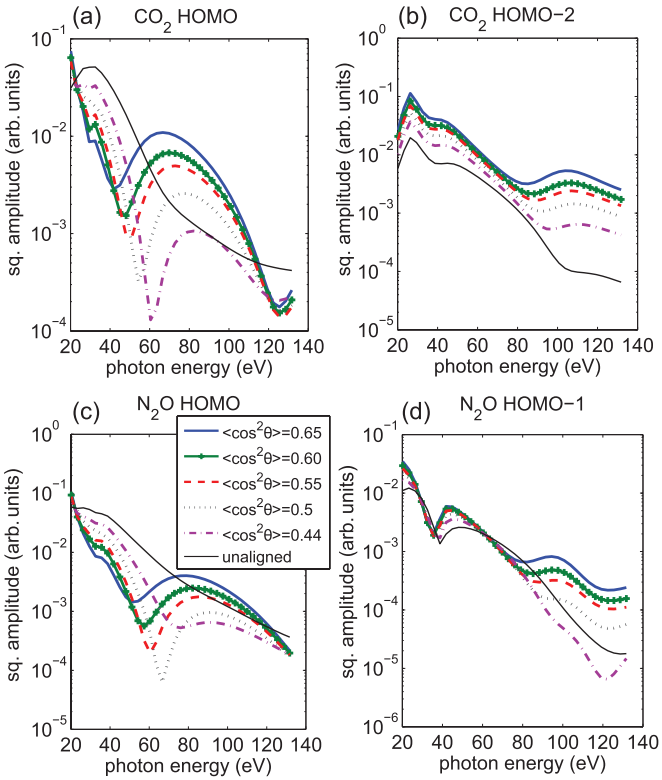

FIG. 14. (Color online) Calculated channel-resolved spectral amplitude of high-harmonic emission obtained by convoluting the product of ionization amplitudes and recombination dipoles with different axis distributions, characterized by $\langle\cos^2\theta\rangle$ given in the legend. Panels (a) and (b) show emission from HOMO and HOMO-2 of CO_2, respectively. Panels (b) and (c) show the emission from HOMO and HOMO-1 in N_2O, respectively.

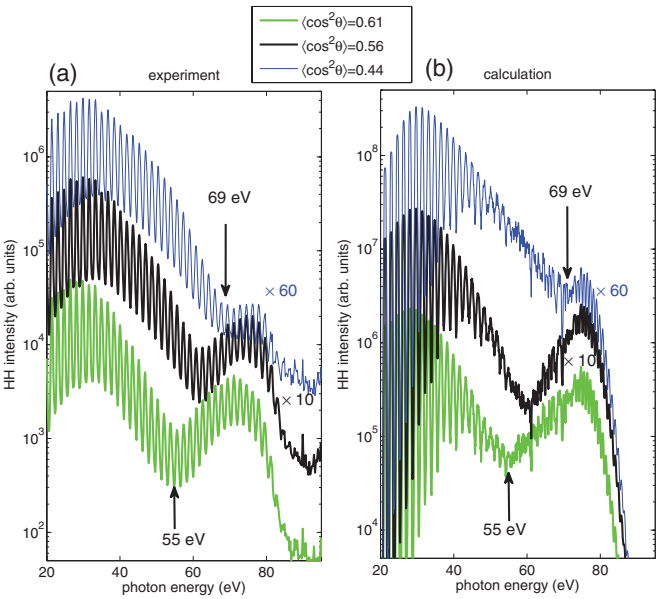

FIG. 15. (Color online) Dependence of the position of the minimum on the degree of alignment. Panel (a) shows measured scaled high-harmonic spectra generated in transiently aligned N_2O using an alignment pulse with intensities from 1.5×10^{13} W/cm^2 (thick light green line) to 0.5×10^{13} W/cm^2 (thin blue line) and a generating pulse of central wavelength 1.46 μm and intensity 0.98×10^{14} W/cm^2. Panel (b) shows the calculated scaled high-harmonic spectra reproducing the experimental high-harmonic spectra from panel (a). The results show that the spectral minimum measured in N_2O is located at higher photon energy for low degrees of alignment.

which suppresses the emission from HOMO in the cutoff and favors the observation of interference with the emission from HOMO-2 at low intensities of the driving field. In our measurements at 1.36 μm the degree of alignment was higher ($\langle\cos^2\theta\rangle = 0.54 \pm 0.01$), which explains the absence of intensity dependence and allows us to attribute the minimum that we observe to the electronic structure of the CO_2 molecule.

A similar trend is also found for N_2O molecules. The general behavior of the emitted spectra from HOMO and HOMO-1 is similar to CO_2. For the same degrees of alignment the minimum in the HOMO emission of N_2O molecules is 10 eV higher (50–70 eV) than in CO_2 (40–60 eV) (Fig. 14). Moreover, the suppression of HOMO emission at photon energies above the minimum with decreasing degree of alignment is less pronounced and more similar to the suppression of the emission from HOMO-1. This aspect enables the observation of a dynamical minimum at higher degrees of alignment compared to CO_2 because the HOMO-1 emission is comparable in intensity to the HOMO emission even for higher degrees of alignment. A dynamical signature can indeed be observed at 1.2 μm, even for high degrees of alignment ($\langle\cos^2\theta\rangle = 0.65$), as demonstrated in our calculations in Fig. 13 and in our measurements in Fig. 5.

The shift of the minimum position with a changing degree of alignment is confirmed experimentally in Fig. 15, which shows high-harmonic spectra of aligned N_2O molecules. Panel (a) shows the experimental high-harmonic spectra, generated using a pulse with a fixed intensity and central wavelength of 1.46 μm, and an alignment pulse with different intensities, ranging from 1.5×10^{13} W/cm^2 (thick green line) to 0.5×10^{13} W/cm^2 (thin blue line). The minimum is found to shift from 55 to 69 eV over this range of pump pulse intensities. The corresponding calculated high-harmonic spectra are shown in panel (b). In these calculations we reproduce the shift of the minimum position in the experimental spectra by only adjusting the axis distribution and obtain degrees of alignment ($\langle\cos^2\theta\rangle$) ranging from 0.44 to 0.61. We thus observe a maximal shift of the minimum position by 14 eV corresponding to a change of $\langle\cos^2\theta\rangle$ by 0.17. We have obtained very similar results for CO_2 with the expected lower degrees of alignment and different absolute positions of the minima.

In summary, dynamic minima can be observed when the emission from lower-lying orbitals becomes comparable to that of the HOMO. This is generally the case in the cutoff as shown in Fig. 11. With increasing wavelength, the plateau of the high-harmonic spectra is extended and the width of the cutoff region is decreased. Thus, contributions from lower-lying orbitals can be expected to be important over a range of harmonics when a generating pulse with short wavelength is used. We expect these results to be general. In the specific case of CO_2, a low degree of alignment tends to favor the observation of dynamic minima by suppressing the emission from HOMO more than that of HOMO-2 in the spectral region beyond the structural minimum. An intensity dependence of

the minimum in CO_2 has thus been observed in high-harmonic spectra generated at 1.17 μm because the degree of alignment and the driving intensity were such that the emissions from HOMO and HOMO-2 were of comparable amplitude in the cutoff. The same is true for N_2O, but occurred even at a higher degree of alignment, because of the less pronounced alignment dependence of the emission intensity.

VI. CONCLUSIONS

In conclusion, we have presented high-harmonic spectra of transiently aligned CO_2 and N_2O molecules in the range of 1.17 to 1.46 μm, combined with a theoretical model that reproduces the observed spectral features. Our experimental results have bridged the wavelength gap between previous measurements of CO_2. We have investigated the effect of different experimental parameters on the position of the spectral minima in CO_2 and N_2O molecules. An intensity dependence of the position of the minimum is present only in the high-harmonic spectra generated under conditions where the minimum is located close to the cutoff of the spectrum, and the emission from HOMO-2 in CO_2 (or HOMO-1 in N_2O) interferes with the emission from HOMO. Our simulations show that the combined effects of a short central wavelength and a relatively low degree of alignment favor the observation of a dynamical minimum. The minima observed in CO_2 spectra generated at 1.36 and 1.46 μm are independent of the intensity of the generating laser pulses. The disappearance of the intensity dependence of the minimum in N_2O takes place for longer wavelengths than in CO_2 owing to the smaller difference in the binding energies of the two dominant orbitals (3.5 eV in N_2O and 4.3 eV in CO_2). Therefore, we can identify the minima observed at 1.46 μm as signatures of the electronic structure of the respective HOMOs. We have recently exploited this fact to show that the different minimum positions for identical axis distributions reflect the different positions of the nodal plane in the HOMO of CO_2 and N_2O molecules [42]. In the present detailed experimental and theoretical study we have demonstrated how to distinguish multielectron from structural effects in high-harmonic spectra. These results advance the understanding of high-harmonic spectroscopy and will be useful in time-resolved applications, such as attosecond measurements of electronic and nuclear dynamics.

ACKNOWLEDGMENTS

We gratefully acknowledge funding from the Swiss National Science Foundation (PP00P2_128274), ETH Zürich (ETH-33 10-3 and Postdoctoral Fellowship Program), and the Marie Curie COFUND program.

[1] J. Itatani, J. Levesque, D. Zeidler, H. Niikura, H. Pépin, J. C. Kieffer, P. B. Corkum, and D. M. Villeneuve, Nature (London) **432**, 867 (2004).
[2] T. Kanai, S. Minemoto, and H. Sakai, Nature (London) **435**, 470 (2005).
[3] S. Baker, J. S. Robinson, C. A. Haworth, H. Teng, R. A. Smith, C. C. Chirila, M. Lein, J. W. G. Tisch, and J. P. Marangos, Science **312**, 424 (2006).
[4] W. Li, X. Zhou, R. Lock, S. Patchkovskii, A. Stolow, H. C. Kapteyn, and M. M. Murnane, Science **322**, 1207 (2008).
[5] H. J. Wörner, J. B. Bertrand, D. V. Kartashov, P. B. Corkum, and D. M. Villeneuve, Nature (London) **466**, 604 (2010).
[6] H. J. Wörner, J. B. Bertrand, B. Fabre, J. Higuet, H. Ruf, A. Dubrouil, S. Patchkovskii, M. Spanner, Y. Mairesse, V. Blanchet *et al.*, Science **334**, 208 (2011).
[7] C. Vozzi, M. Negro, F. Calegari, G. Sansone, M. Nisoli, S. De Silvestri, and S. Stagira, Nat. Phys. **7**, 822 (2011).
[8] J. P. Farrell, S. Petretti, J. Förster, B. K. McFarland, L. S. Spector, Y. V. Vanne, P. Decleva, P. H. Bucksbaum, A. Saenz, and M. Gühr, Phys. Rev. Lett. **107**, 083001 (2011).
[9] T. Morishita, A.-T. Le, Z. Chen, and C. D. Lin, Phys. Rev. Lett. **100**, 013903 (2008).
[10] H. J. Wörner, H. Niikura, J. B. Bertrand, P. B. Corkum, and D. M. Villeneuve, Phys. Rev. Lett. **102**, 103901 (2009).
[11] A.-T. Le, R. R. Lucchese, S. Tonzani, T. Morishita, and C. D. Lin, Phys. Rev. A **80**, 013401 (2009).
[12] A.-T. Le, R. R. Lucchese, M. T. Lee, and C. D. Lin, Phys. Rev. Lett. **102**, 203001 (2009).
[13] M. Lein, N. Hay, R. Velotta, J. P. Marangos, and P. L. Knight, Phys. Rev. Lett. **88**, 183903 (2002).
[14] B. K. McFarland, J. P. Farrell, P. H. Bucksbaum, and M. Gühr, Science **322**, 1232 (2008).
[15] W. Boutu, S. Haessler, H. Merdji, P. Breger, G. Waters, M. Stankiewicz, L. J. Frasinski, R. Taieb, J. Caillat, A. Maquet *et al.*, Nat. Phys. **4**, 545 (2008).
[16] O. Smirnova, Y. Mairesse, S. Patchkovskii, N. Dudovich, D. M. Villeneuve, P. B. Corkum, and M. Y. Ivanov, Nature (London) **460**, 972 (2009).
[17] S. Haessler, J. Caillat, W. Boutu, C. Giovanetti-Teixeira, T. Ruchon, T. Auguste, Z. Diveki, P. Breger, A. Maquet, B. Carre *et al.*, Nat. Phys. **6**, 200 (2010).
[18] H. J. Wörner, J. B. Bertrand, P. Hockett, P. B. Corkum, and D. M. Villeneuve, Phys. Rev. Lett. **104**, 233904 (2010).
[19] R. Torres, T. Siegel, L. Brugnera, I. Procino, J. G. Underwood, C. Altucci, R. Velotta, E. Springate, C. Froud, I. C. E. Turcu *et al.*, Phys. Rev. A **81**, 051802 (2010).
[20] Y.-C. Han and L. B. Madsen, J. Phys. B **43**, 225601 (2010).
[21] A. D. Shiner, B. Schmidt, C. Trallero-Herrero, Wörner, S. Patchkovskii, P. B. Corkum, J.-C. Kieffer, F. Légaré, and D. M. Villeneuve, Nat. Phys. **7**, 464 (2011).
[22] G. N. Gibson and R. R. Freeman, Phys. Rev. Lett. **67**, 1230 (1991).
[23] T. Kanai, E. J. Takahashi, Y. Nabekawa, and K. Midorikawa, Phys. Rev. Lett. **98**, 153904 (2007).
[24] C. Vozzi, F. Calegari, E. Benedetti, J.-P. Caumes, G. Sansone, S. Stagira, M. Nisoli, R. Torres, E. Heesel, N. Kajumba *et al.*, Phys. Rev. Lett. **95**, 153902 (2005).
[25] K. Kato, S. Minemoto, and H. Sakai, Phys. Rev. A **84**, 021403 (2011).
[26] J. Muth-Böhm, A. Becker, and F. H. M. Faisal, Phys. Rev. Lett. **85**, 2280 (2000).
[27] A. Jaron-Becker, A. Becker, and F. H. M. Faisal, J. Phys. B **36**, L375 (2003).

[28] V. S. Yakovlev, M. Ivanov, and F. Krausz, Opt. Express **15**, 15351 (2007).
[29] K. Kimura, S. Katsumata, Y. Achiba, T. Yamazaki, and S. Iwata, *Handbook of HeI Photoelectron Spectra* (Japan Scientific Societies Press, Tokyo, 1981).
[30] S. Patchkovskii, Z. Zhao, T. Brabec, and D. M. Villeneuve, Phys. Rev. Lett. **97**, 123003 (2006).
[31] R. Santra and A. Gordon, Phys. Rev. Lett. **96**, 073906 (2006).
[32] S. Patchkovskii, Z. Zhao, T. Brabec, and D. M. Villeneuve, J. Chem. Phys. **126**, 114306 (2007).
[33] M. Y. Ivanov, T. Brabec, and N. Burnett, Phys. Rev. A **54**, 742 (1996).
[34] A.-T. Le, R. R. Lucchese, and C. D. Lin, J. Phys. B **42**, 211001 (2009).
[35] S. Petretti, Y. V. Vanne, A. Saenz, A. Castro, and P. Decleva, Phys. Rev. Lett. **104**, 223001 (2010).
[36] I. Thomann, R. Lock, V. Sharma, E. Gagnon, S. T. Pratt, H. C. Kapteyn, M. M. Murnane, and W. Li, J. Phys. Chem. A **112**, 9382 (2008).
[37] D. Pavičić, K. F. Lee, D. M. Rayner, P. B. Corkum, and D. M. Villeneuve, Phys. Rev. Lett. **98**, 243001 (2007).
[38] G. L. Yudin and M. Y. Ivanov, Phys. Rev. A **64**, 013409 (2001).
[39] F. A. Gianturco, R. R. Lucchese, and N. Sanna, J. Chem. Phys. **100**, 6464 (1994).
[40] A. P. P. Natalense and R. R. Lucchese, J. Chem. Phys. **111**, 5344 (1999).
[41] A. Rupenyan, J. B. Bertrand, D. M. Villeneuve, and H. J. Wörner, Phys. Rev. Lett. **108**, 033903 (2012).
[42] A. Rupenyan, P. M. Kraus, J. Schneider, and H. J. Wörner, Phys. Rev. A **87**, 031401(R) (2013).
[43] M. Abu-samha and L. B. Madsen, Phys. Rev. A **82**, 043413 (2010).
[44] X. Zhu, Q. Zhang, W. Hong, P. Lan, and P. Lu, Opt. Express **19**, 436 (2011).
[45] B. B. Augstein and C. F. de Morisson Faria, J. Phys. B **44**, 055601 (2011).
[46] A. Etches, M. B. Gaarde, and L. B. Madsen, Phys. Rev. A **84**, 023418 (2011).
[47] C. Jin, A.-T. Le, and C. D. Lin, Phys. Rev. A **83**, 053409 (2011).